nature photonics

SUPPLEMENTARY INFORMATION

DOI: 10.1038/NPHOTON.2017.82

In the format provided by the authors and unedited.

Compressive hyperspectral time-resolved wide-field fluorescence lifetime imaging

Qi Pian, Ruoyang Yao, Nattawut Sinsuebphon, Xavier Intes*

*Biomedical Engineering Department, Rensselaer Polytechnic Institute, 110 8th St. Troy, NY 12180, USA.

E-mail: intesx@rpi.edu

Supplementary Information

A. Hyperspectral wide-field single-pixel TD-MFLI system

A detailed description of the system implementation is provided here. Fig. S1a shows a diagram of the system configuration without the light source (Mai Tai HP, Spectral Physics, CA) while Fig. S1b shows the corresponding physical implementation of the system. The Ti:Sapphire laser is capable of generating 80 MHz excitation light pulses from 690 nm to 1040 nm with ~100 fs pulse width and up to 3 Watts of power at 800 nm (~0.9 Watt at 695 nm). The excitation light power is controlled and monitored by a variable attenuator (CCVA-TL-KT, Newport Corporation, CA) before injection into a multimode fibre (P400-10-VIS-NIR, NA= 0.22, Ocean Optics Inc., FL). The input can be switched between transmission and reflectance geometries by coupling into either DMD I or DMD II. In transmission geometry, the incoming laser light is first collimated by a fibre collimator C1 (F810SMA-780, Thorlabs Inc, NJ) and is then focused using a f= 25.4 mm lens L1 (LB1761-B, Thorlabs Inc, NJ) into the integrator rod of the DMD I optics (D4110 plus S2+ VIS optics module, f/2.6~2.9, with a 9-mm spacer ring added to the projection lens to increase focus range of the optical module, Digital Light Innovations, TX). In the reflectance geometry, the incoming light is collimated using collimator C2 (F220SMA-B, Thorlabs Inc, NJ) and then coupled into DMD II (Pico Projector PK101, Optoma USA, CA) (LED and coupling lens removed). It is possible to achieve up to ~10 mW/cm^2 illumination power density within the FOV. On the detection side, the emitted signal collected by DMD III (D4110 plus S2+ NIR optics module, f/2.6~2.9, with an 8.6-mm spacer ring added to the objective to increase focus range, Digital Light Innovations, TX) is then focused into a light guide (11 mm fibre bundle, 200 µm core diameter of single fibre, NA= 0.22) with lens group I (from left to right in Fig. S1a, L2, L3: f= 30.0 mm, AC254-030-B, Thorlabs; L4: f= 40.0 mm, #48-769, Edmund Optics), lens group II (replacing the original relay lenses, from left to right in Fig. S1a, L5: f= 30 mm, LB1757-B, Thorlabs Inc, NJ; L6, L7: f= 25.4 mm, LB1761-B, Thorlabs Inc, NJ), and a light-homogenizing transmission integrator rod (#63-086 Hexagonal Light Pipe, Edmund Optics, NJ) between them. A long-pass filter (FF01-715/LP-25, Semrock, NY) is used to block the excitation light. Overall, ROIs on the imaging plate are demagnified ~16.5 (for *in vitro* studies) or ~18.9 (for *in vivo* studies) times by the detection optics. Finally, the light guide converts a 3-mm-diameter circular aperture to a 1mm×7mm linear aperture for input to a time-resolved spectrophotometer (MW-FLIM, f/3.7, Becker & Hickl GmbH, Germany). The spectrophotometer employs a 1200 lines/mm blazed grating G (#77412, 750 nm blaze, Newport Optics, CA) and two concave mirrors (M2 and M3) to achieve ~5.2 nm/mm dispersion. Data acquisition of the multi-anode PMT detector (PML-16-C, Becker & Hickl GmbH, Germany) is achieved with SPC-150, DCC-100 control modules (Becker & Hickl GmbH, Germany) based on the time-correlated single photon counting (TCSPC) technique and 4 channel bits are applied in the detector to encode 16 wavelength channels.

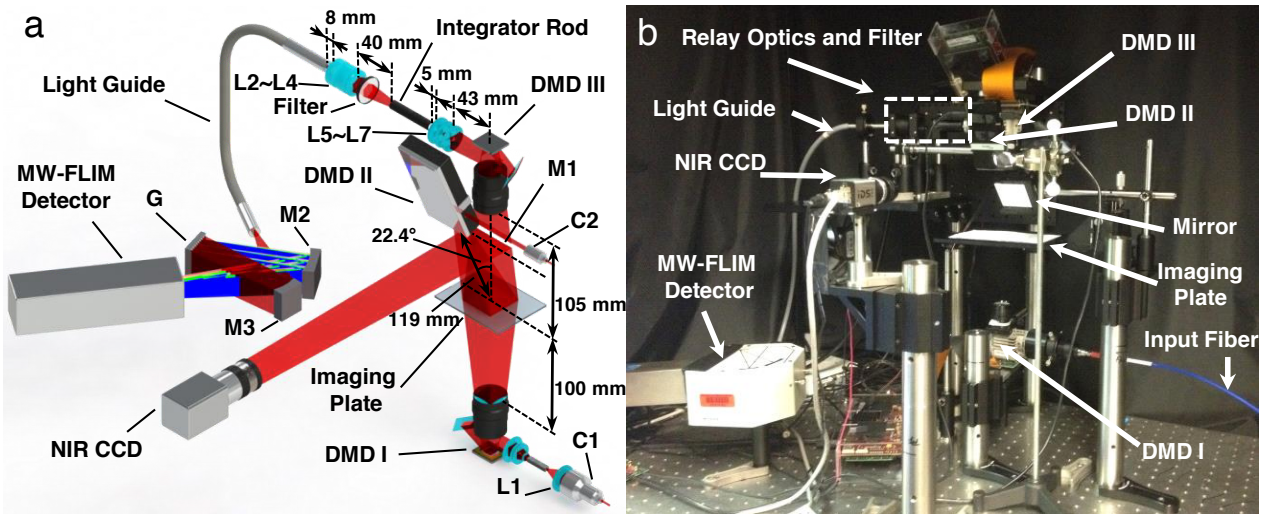

Figure S1 | Diagram and picture of the imaging system setup. **a**, A detailed diagram of the system configuration (Mai Tai laser not shown here). **b**, A picture of the physical implementation of the imaging platform. Lenses: L1 (f= 25.4 mm), L2 (f= 30.0 mm), L3 (f= 30.0 mm), L4 (f= 40.0 mm), L5 (f= 30.0 mm), L6 (f= 25.4 mm), L7 (f= 25.4 mm); Fibre collimators: C1 and C2; Grating: G (1200 lines/mm, 750 nm blaze); Mirrors: M1, M2 and M3.

B. Data processing

An intensity threshold was applied to the hyperspectral time-resolved reconstructed images to select the regions of interest (ROIs). Each TPSF curve was first processed with the Anscombe transform to stabilize Poisson noise variance, then denoised with a Gaussian filter and normalized to its peak before bi-exponential lifetime fitting. The model used for bi-exponential lifetime fittings is: $TPSF = IRF * [A_1\exp(-t/\tau_1) + A_2\exp(-t/\tau_2)]$, $(A_1 + A_2 = 1)$, where $TPSF$ is temporal point spread function, IRF is instrumental response function, τ_1 and τ_2 are short and long lifetime components, A_1 and A_2 are the corresponding fractions of these two components. The symbol '$*$' represents convolution here. When retrieving the mean lifetimes, fitting ranges for τ_1 and τ_2 were set to 0.40 ± 0.20 ns and 0.80 ± 0.30 ns. In terms of estimating FRETing donor fraction (FD%), the fitting ranges for short (FRETing donor) and long lifetime (non-FRETing donor) components were set as 0.25 ± 0.03 ns, 1.05 ± 0 ns respectively for both *in vitro* and *in vivo* studies based on calibration. An example of bi-exponential fitting of an experimental TPSF is shown in Fig. S2.

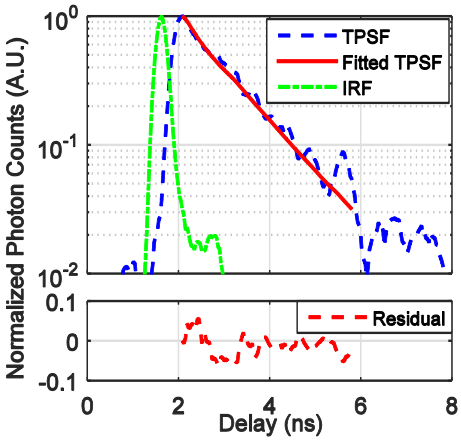

Figure S2 | Examples of bi-exponential lifetime fitting. The fitting result and residual of a pixel in the mouse liver using the bi-exponential fitting method (725 nm channel) in order to retrieve FD%.

C. The comparison between spatial multiplexing single-pixel method and ICCD-based method

In this paper, we reported a novel approach to perform multi-spectral macroscopic fluorescence lifetime imaging and benchmarked it with our well-established gated ICCD system that has been used extensively for *in vitro* and *in vivo* FRET studies[1–3]. The quantitative comparison was performed in the context of lifetime-based parameter estimation with special focus on the FD% as it is one of the most challenging parameters to obtain robustly and accurately in FRET applications[4,5]. It is important to note that our single-pixel imaging platform is still not yet optimized in terms of acquisition speed and we expect significant acquisition speed-up improvements in the near future by using appropriate data reduction techniques and a new generation of time-resolved detectors with enhanced sensitivity. Additionally, the performances of the single-pixel and the gated-ICCD systems are affected by several key factors such as temporal resolution (~150 ps for the single-pixel MFLI system and 300 ps for the ICCD-based system if calculated as full width at half maximum of IRF), temporal gating (32.6 ps temporal channel width for the single-pixel MFLI system and 300 ps gate width for the ICCD-based system), f-number of collecting optics (f-number> 3.7 for the single-pixel MFLI system and f-number= ~1.8 for the ICCD-based system), photocathode quantum efficiency at the NIR wavelength range, field of view (FOV) and spatial resolution.

D. The comparison between spatial multiplexing single-pixel method and raster scanning method

Considering the difficulty to concurrently implement raster scanning based on galvo-mirrors in the proposed system, we employed scan-mimicking point scan patterns (scanning point size was the same as the minimum element size of Hadamard patterns) to compare the Hadamard pattern-based single-pixel MFLI and the raster scanning method. This experimental study was performed as follows: unconjugated Alexa Fluor 750 (A33085, Thermo Fisher Scientific, MA) buffered by PBS was filled in 9 wells of a 96-well plate (2.08 μM concentration, 250 μL volume for each well). The sample was excited at 740 nm and the emission light was detected after a band-pass emission filter (FF01-780/12-25, Semrock, NY) in both methods. The signals from 777.4 nm (emission peak channel) were analyzed. The ROI areas for both techniques were 35 × 35 mm^2. For the spatial multiplexing MFLI method, the sample was imaged using 1024 Hadamard patterns (32 × 32 resolution, 1.09 × 1.09 mm^2 pixel size on the imaging plate) in total with 1 s exposure time per pattern and ~1.85 mJ/cm^2 illumination energy density per measurement (948.74 mJ/cm^2 energy density over the whole imaging process considering the 50% fill factor of Hadamard patterns). Time-resolved fluorescence intensity distribution of the sample $f_{Had}(x, y, t)$ (x, y are spatial domain coordinates: x, y = 1, 2…32; t is the time domain coordinate) was recovered by solving the inverse problem mentioned in the main text. For the raster scanning method, the scanning point was set to the same size as in the Hadamard pattern-based method (1.09 × 1.09 mm^2) in order to maintain spatial resolution for comparison. Scanning was simulated with the illumination DMD by turning micro-mirrors within one 'pixel' (1.09 × 1.09 mm^2 projection size on the imaging plate) into the "ON" state at a time and time-resolved fluorescence intensity distribution $f_{Scan}(x, y, t)$ (x, y = 1, 2…32; t is the time domain coordinate) was generated after 1024 scans. Different illumination energy densities per measurement range from ~1.85 mJ/cm^2 to 27.80 mJ/cm^2 were applied in the scanning technique by tuning the laser power and exposure time (see Tab. S1 for illumination energy density and exposure time settings for each imaging experiment). Both methods provided time-resolved fluorescent images of 1024 pixels (32 × 32 resolution).

All signals from one well based on the raster scanning method (Scan 4 in Tab. S1) were added together to form a

ground truth, and MSE (mean square error) for the TPSF of each pixel (1.09 × 1.09 mm^2) and average MSE across the whole ROI were calculated according to this ground truth for every imaging condition (see Fig. S3 a-f and Fig. S4 a). In addition, reconstructed f_{Had} and f_{Scan} were filtered (filter size and standard deviation were kept constant for all conditions) and fitted to a mono-exponential decay model (initial lifetime for fitting: 0.45 ns, lifetime fitting range: ±0.1 ns) to retrieve the mean and standard deviation values of fluorescence lifetime under each imaging condition (see Fig. S4 b). The comparison shows the improvements in SNR (signal-to-noise ratio) and quantification accuracy of lifetime estimation induced by the implementation of Hadamard patterns in single-pixel MFLI. This is expected as Hadamard multiplexing is suppressing additive noise and background stray light, as reported by L. Streeter et. al[6]. The overall illumination energy dose deposited on the sample for Hadamard multiplexing could be further reduced by compressive sensing[7] methodologies aiming at decreasing the required measurement number.

Table S1 | Illumination energy density (per measurement) settings for different experiments

	Had	Scan1	Scan2	Scan3	Scan4
Power Density (mW/cm^2)	1.85	1.85	5.56	5.56	5.56
Exposure time (s)	1	1	2	3	5
Energy Density (mJ/cm^2)	1.85	1.85	11.12	16.68	27.80

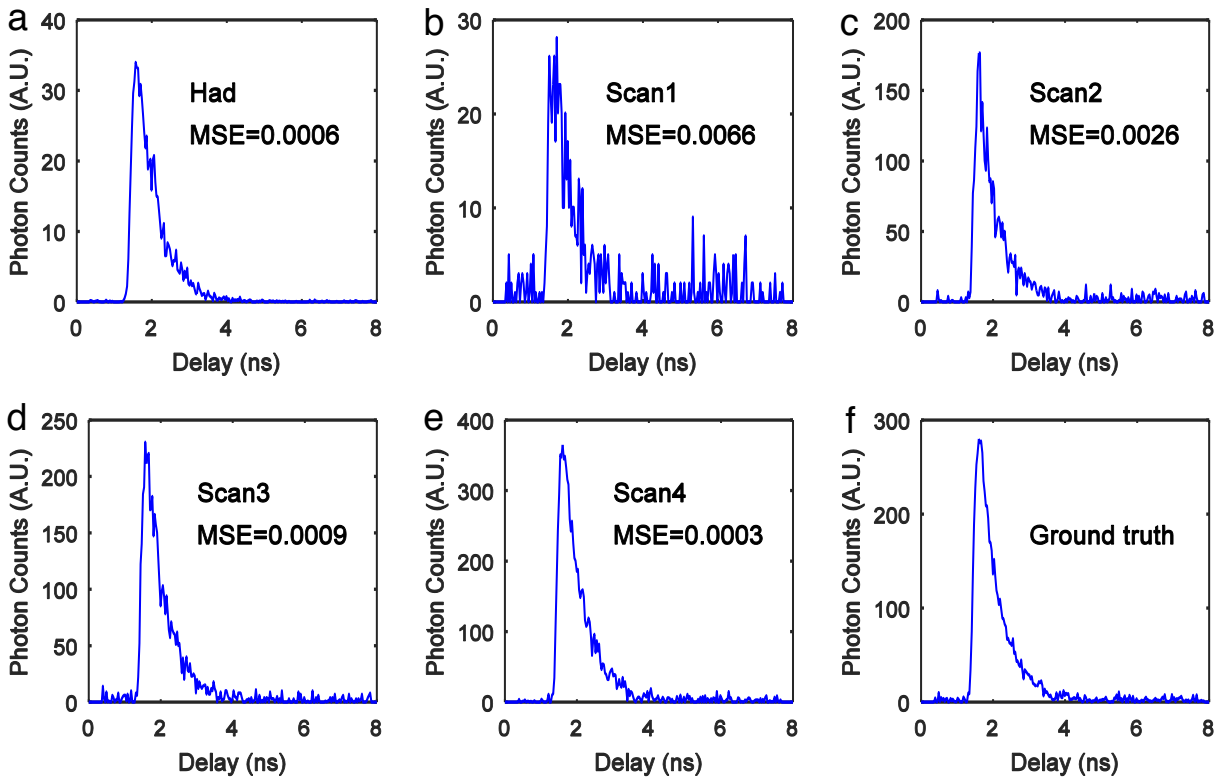

Figure S3 | TPSFs for the same pixel that were obtained with five different imaging conditions and their MSEs calculated for each case compared to the ground truth (channel center wavelength: 777.4 nm). TPSFs and their MSEs obtained with **a,** 'Had'; **b,** 'Scan1'; **c,** 'Scan2'; **d,** 'Scan3' and **e,** 'Scan4' methods described in **Tab. S1**. **f,** The ground truth used to calculate the MSEs (obtained by averaging TPSFs within the same well using method 'Scan4').

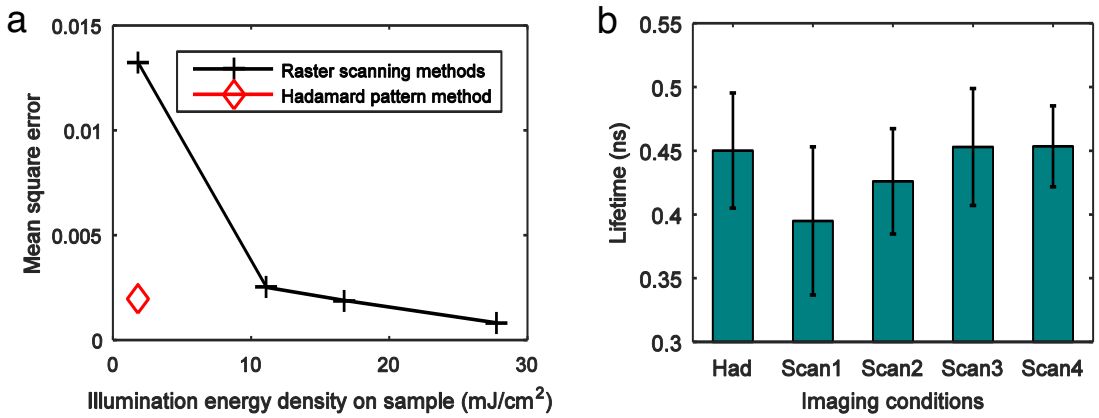

Figure S4 | Quantification study results calculated within the ROIs of each imaging condition. a, The average MSEs of all TPSFs calculated within the ROI of each imaging condition. **b,** The mean and standard deviation values of fluorescence lifetime calculated within the ROI of each imaging condition. The mean and standard deviation values of lifetime obtained from the five conditions are: 0.450±0.045 ns, 0.395±0.058 ns, 0.426±0.041 ns, 0.453±0.046 ns, 0.453±0.032 ns.

References

1. Venugopal, V., Chen, J. & Intes, X. Development of an optical imaging platform for functional imaging of small animals using wide-field excitation. *Biomed. Opt. Express* **1,** 143–156 (2010).
2. Venugopal, V., Chen, J., Barroso, M. & Intes, X. Quantitative tomographic imaging of intermolecular FRET in small animals. *Biomed. Opt. Express* **3,** 3161–3175 (2012).
3. Zhao, L. *et al.* Spatial light modulator based active wide-field illumination for *ex vivo* and *in vivo* quantitative NIR FRET imaging. *Biomed. Opt. Express* **5,** 944–960 (2014).
4. Omer, T., Zhao, L., Intes, X. & Hahn, J. Reduced temporal sampling effect on accuracy of time-domain fluorescence lifetime Förster resonance energy transfer. *J. Biomed. Opt.* **19,** 086023 (2014).
5. Chen, S.-J., Sinsuebphon, N. & Intes, X. Assessment of Gate Width Size on Lifetime-Based Förster Resonance Energy Transfer Parameter Estimation. *Photonics* **2,** 1027–1042 (2015).
6. Streeter, L., Burling-Claridge, G. R., Cree, M. J. & Künnemeyer, R. Optical full Hadamard matrix multiplexing and noise effects. *Appl. Opt.* **48,** 2078–2085 (2009).
7. Studer, V. *et al.* Compressive fluorescence microscopy for biological and hyperspectral imaging. *Proc. Natl. Acad. Sci. U. S. A.* **109,** E1679–E1687 (2012).